Received 8 May 2024; revised 22 July 2024; accepted 14 August 2024. Date of publication 16 August 2024; date of current version 24 September 2024.

Digital Object Identifier 10.1109/OJAP.2024.3445300

Ascertaining Operating Points of Harmonic Transponders Using Intermodulation Responses

JEFF FROLIK (Senior Member, IEEE), ELSIE ANTHONIO (Student Member, IEEE), RYE FOUGHT (Student Member, IEEE), AND TARA HARTE (Student Member, IEEE)

Department of Electrical and Biomedical Engineering, University of Vermont, Burlington, VT 05405, USA

CORRESPONDING AUTHOR: J. FROLIK (e-mail: jfrolik@uvm.edu)

This work was supported by the USDA National Institute of Food and Agriculture under Grant 2023-67022-38830.

ABSTRACT Harmonic transponders are nonlinear, passive devices that typically receive an interrogation signal at one single frequency and reradiate harmonics. In this work, we propose leveraging the device's nonlinearity by interrogating with two closely spaced signals and then measuring the second harmonics and nearby second and fourth intermodulation distortion products. Our results show that we are able to remotely determine the power incident at the device, over a 25 dB range and within ± 1 dB, using only the relative ratios between these received components. This result has applications in characterizing the loss of unknown channels and in conducting over-the-air characterization of fully integrated transponders. We demonstrate this latter application.

INDEX TERMS Harmonic transponders, intermodulation products, microwave devices, microwave measurements, nonlinear circuits.

I. INTRODUCTION

HARMONIC transponders are passive wireless devices that have been investigated for a variety of novel purposes, including tracking of insects [1], locating buried infrastructure [2], and monitoring temperature [3] and humidity [4]. These devices are relatively simplistic, consisting of receive and transmit antennas, along with a diode, whose nonlinearity produces harmonics. Fig. 1 shows an example harmonic transponder, which was designed to receive a signal at $f = \sim$890 MHz and reradiate (i.e., backscatter) a second harmonic, $2f$ (i.e., at $\sim$1.78 GHz, in this case) [5].

A significant advantage of harmonic transponders, compared to a mono-frequency transponders (e.g., RFID tags), is that backscatter and ground clutter interference are effectively eliminated, since the interrogator is tuned to receive only the harmonic tone of interest. Also, harmonic transponders have activation powers nearly 20 dB below that of RFIDs (i.e., <-30 dBm [6]), and therefore are able to be interrogated at greater distances [7], at lower power, and/or while embedded in a media that can significantly attenuate the interrogation signal (e.g., soil).

For the applications noted above, the parameter of interest is either the transponder's *point* of location or a measurement of a physical property at that *point* (e.g., temperature). However, for other applications, the parameter of interest could be related to the *channel* between the interrogator and the transponder. Such an example is ascertaining soil moisture by determining the channel's loss on the forward and/or reverse links [8]. In this work, we present a method that allows one to *remotely* determine the incident power at the harmonic transponder. This ability allows one to determine the loss of an unknown channel or characterize the harmonic transponder through over-the-air (OTA) testing.

The unique contributions of the work are twofold. First, leveraging intermodulation distortion products, we propose an OTA method to discern the operating point of an embedded harmonic transponder. Second, we show that knowing the operating point will allow one to characterize the individual components of the device's overall response. The method also has applications in determining the propagation loss of an unknown channel.

II. HARMONIC TRANSPONDER INTERROGATION

A representative interrogation system for a harmonic transponder is illustrated in Fig. 2. An interrogator sends a signal of known frequency (f) and power and measures the power of the backscattered harmonic ($2f$). The power

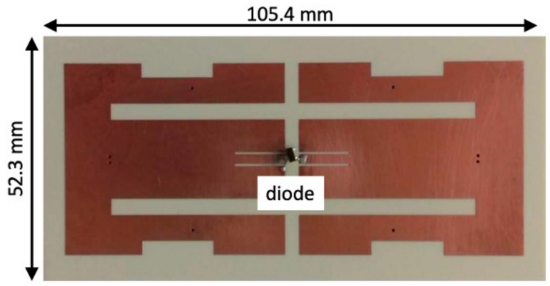

FIGURE 1. Example harmonic transponder that receives an interrogation signal at ~890 MHz and backscatters a second harmonic [5].

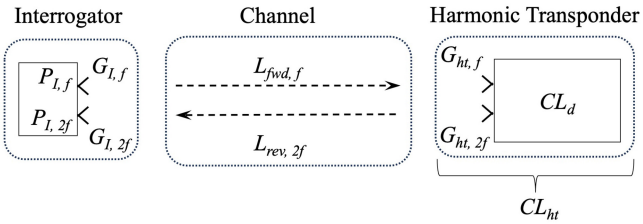

FIGURE 2. The harmonic transponder systems consists of an interrogator, forward and reverse links, and the harmonic transponder. The transmitted and received power by the interrogator are given by $P_{I,f}$ and $P_{I,2f}$, respectively. The interrogator's transmit and receive antenna gains are $G_{I,f}$ and $G_{I,2f}$, respectively. Forward and reverse link losses are $L_{fwd,f}$ and $L_{rev,2f}$, respectively. The total conversion loss of the harmonic transponder (CL_{ht}) is given by its receive and transmit antenna gains ($G_{ht,f}$ and $G_{ht,2f}$, respectively) and the diode's conversion loss (CL_d), which is *nonlinear*.

of the received backscattered signal ($P_{I,2f}$), is dependent on the interrogator's effective isotropic radiated power ($EIRP = P_{I,f} \times G_{I,f}$), the forward link loss ($L_{fwd,f}$), the harmonic transponders's conversion loss ($CL_{ht} = G_{ht,f} \times CL_d \times G_{ht,2f}$), the reverse link loss ($L_{rev,2f}$), and interrogator's receive antenna gain ($G_{I,2f}$), as shown (in log form) in Eq. (1).

$$P_{I,2f} = EIRP - L_{fwd,f} - \underbrace{CL_{ht}}_{nonlinear} - L_{rev,2f} + G_{I,2f} \quad (1)$$

Note that as the harmonic transponder's conversion loss, the power ratio of the incident signal at f to the reradiated signal at $2f$ (CL_{ht}), is *nonlinear*, for the device diode's conversion loss (CL_d) has nonlinear dependency on its incident power. Thus the reradiated signal at $2f$ has a *nonlinear* dependency on changes in forward link, i.e., $EIRP$, loss (L_{fwd}) and/or the device's orientation (impacting $G_{ht,f}$). At the same time, the received backscatter power depends *linearly* on the device's transmit antenna gain/orientation ($G_{ht,2f}$) and the reverse link (i.e., $G_{I,2f}$, $L_{rev,2f}$).

Typically, the performance of a harmonic transponder is characterized using a *single*-carrier test to ascertain the device conversion loss (CL_{ht}). Through such testing, harmonic transponder conversion loss has been shown to not only be a function of incident power, but also the interrogation frequency and the device's orientation [9], [10]. As will be shown shortly in this current work, additional and more accurate information can be obtained using a *two*-carrier approach. While two-carrier testing has been used for characterizing RFIDs in order to mitigate self-interference [11], [12], to the authors' knowledge, the current work is the first to employ this technique for harmonic transponders.

For a given measurement, there should be certain knowns that appear in Eq. (1). Particularly, the performance of the interrogator should be known, i.e., its $EIRP$ and $G_{I,2f}$. Still, for an OTA measurement, the operating point (OP) for the device, which we define herein as the power incident at a *normally oriented* device, will depend on unknowns, as we show (also in log form) in Eq. (2).

$$OP = EIRP \underbrace{-L_{fwd,f}}_{\text{known?}} + \underbrace{G_{ht,f}}_{\text{orientation certain?}} \quad (2)$$

Under free-space/idealized channel conditions, one can calculate the forward and reverse link losses and determine the OP, if one assumes knowledge of the device's orientation and therefore $G_{ht,f}$. This is the approach used in laboratory testing, such as presented in [13]. However, when the device is embedded in a complex environment with unknown loss (e.g., a multipath channel or in soil) or is placed with unknown orientation in free space, then, using existing methods, one cannot isolate the forward link loss from the device conversion loss or from the reverse link loss. This is particularly true when the media has different loss characteristics at f (forward link) and $2f$ (reverse link), due to the channel's frequency-dependent multipath [14] or its dielectric properties [15].

III. CHARACTERIZING NONLINEARITIES

In this section, we review foundations related to characterizing nonlinear devices, such as amplifiers, in order to provide context for our work with harmonic transponders. For the purpose of this section's discussion, we consider the input a device to be $x(t)$ and its output to be $y(t)$, and assume the units associated with these signals to be volts (V).

A. SINGLE CARRIER METHOD

For a device to be considered *linear*, the following relationship *must* hold,

$$y_L(t) = \alpha x(t - \tau), \quad (3)$$

where α and τ, are amplitude scaling and time delay constants, respectively. Letting the input be a single sinusoid, i.e., $x(t) = Acos(2\pi f_0 t)$, then the output of a linear system will only consist of a single frequency, i.e., one occurring at f_0. In contrast, for *nonlinear* systems, the output takes on the form

$$y_{NL}(t) = \alpha_1 x(t - \tau_1) + \alpha_2 x^2(t - \tau_2) + \alpha_3 x^3(t - \tau_3) + , \ldots , \quad (4)$$

which, when the input is a single sinusoid, results in *harmonic* components potentially at $2f_0$, $3f_0$, etc., in addition

to the one at f_0. We can rewrite the resulting output signal in terms of its Fourier series components.

$$y_{NL}(t) = \sum_{k=0}^{+\infty} A_k cos(2\pi k f_0 t + \theta_k), \tag{5}$$

where A_k, kf_0, and θ_k are the amplitude (V), frequency (Hz) and phase (radians), respectively, of the k^{th} harmonic. For many applications, these additional *distortion* components are undesirable. For example, in low frequency systems, e.g., audio and power, the impact of distortion is quantified as the total harmonic distortion (*THD*), i.e., ratio of the root mean square (RMS) value of the harmonics relative to the fundamental.

$$THD = \frac{\sqrt{A_2^2 + A_3^2 + \cdots}}{A_1} \tag{6}$$

THD is negligible for audio when less than 0.5% [16] and it is recommended to be less than 5% for power systems [17]. However, for microwave frequency systems, harmonics often fall *outside* the measurable bandwidth of the device and thus alternative methods are needed to quantify distortion, i.e., methods which use *inband* information.

B. DUAL CARRIER METHOD

Leveraging intermodulation distortion (IMD) is a well-known approach for characterizing nonlinear devices [18]. In this method, two closely-spaced frequencies (f_1 and f_2), are simultaneously presented, with equal weighting (A), at a device's input, i.e.,

$$x(t) = Acos(2\pi f_1 t) + Acos(2\pi f_2 t). \tag{7}$$

At the output, the result is

$$y_{NL}(t) = \sum_{k=1}^{\infty} C_k \cos(2\pi (m_k f_1 \pm n_k f_2)t + \theta_k), \tag{8}$$

where and $m_k, n_k \in Z^+$ (non-negative integers), and C_k and θ_k are the components amplitude and phase, respectively. When either m or $n = 0$, the output component will be a harmonic of one of the two input frequencies (f_2 or f_1, respectively). Otherwise, the component is an $(m+n)^{th}-$order intermodulation product (IM).

When $|m-n| = 1$, the IM will fall inband with the input frequencies, f_1 and f_2. Of particular interest are the two *third*-order intermodulation products components (IM3), i.e., $2f_1 - f_2$ and $2f_2 - f_1$). The third order intercept (TOI or IP_3) is a common metric used to quantify nonlinearity. IP_3 is the extrapolated point where the output power of the fundamental (i.e., f_1 or f_2 alone) will be equal to the extrapolated power of the IM3 component. For devices where linearity is desired, the higher the IP_3, the better.

IM3 measurements have been leveraged to characterize RFID passive transponders. Using a multistatic interrogation approach, the work in [11] found the device's normalized radiation pattern by measuring the IM3 return frequency (915 MHz), which fell in the same band as f_1 (916 MHz) and f_2 (917 MHz). A similar approach has also been applied for radiation pattern mapping [12]. Conducting these measurements at the IM3 frequency avoided self-jamming that can occur when only a single interrogation frequency is used with RFIDs. This benefit has also been shown for a system that interrogated an RFID operating at 5.8 GHz [19].

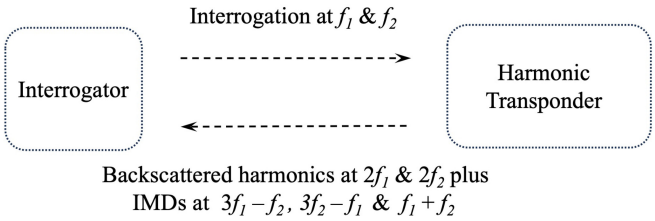

FIGURE 3. Proposed approach in which two tones are used for interrogation, resulting in intermodulation distortion products (IMDs) being returned, in addition to harmonics.

For the harmonics transponders considered herein, their operation depends on being *highly* nonlinear to produce a strong backscattered harmonic response. Furthermore, we are interested in measurable responses at *twice* the interrogation signal, e.g., at $2f_0$. In the next section, we leverage the dual carrier interrogation approach to introduce intermodulation products in this higher band.

IV. DUAL CARRIER INTERROGATION OF HARMONIC TRANSPONDERS

We now present a method for interrogating harmonic transponders, with the objective of determining the power incident at the device, i.e., its operating point (*OP*). The *OP* determines the power seen by the transponder's diode, which is the source of nonlinearity in the system. As we will show, the *remotely* measurable nonlinear behavior caused by the diode can be mapped back its *OP*.

A. APPROACH

As illustrated in Fig. 3, the interrogator transmits two closely-spaced frequencies (f_1 and f_2) and measures the returns at (1) the second harmonics ($2f_1$ and $2f_2$; 2H), (2) the *second*-order IMD products ($f_1 + f_2$; IM2), and (3) the *fourth*-order IMD products ($3f_1 - f_2$ and $3f_2 - f_1$; IM4). For the device seen in Fig. 1, Fig. 4 shows these components in remotely-measured, backscattered response, i.e., the spectrum received by the interrogator.

The spectrum seen in Fig. 4 is for a fixed transmitted power. In Fig. 5, we show the response of the these components as a function of the device's *OP*. In these data, the forward and reverse channel losses have calibrated out, so these axes show device's *OP* ($x-$axis) and radiated component power ($y-$axis).

Note that the *relative* power ratios between these three distortion components, as measured by the interrogator, change with the power incident at the device and thus provide a unique signature of the device's *OP*. That is, these

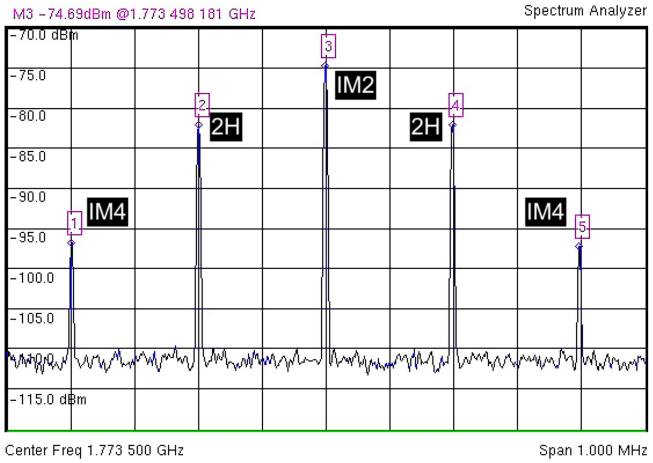

FIGURE 4. Remotely measured signal with 2nd harmonics (2H = 1,773.3 MHz & 1,775.7 MHz), 2nd order IM (IM2 = 1,773.5 MHz), and 4th order IMs (IM4 = 1,773.1 MHz & 1,773.9 MHz). IM2-$\overline{2H}$= 7.6 dB and IM2-$\overline{IM4}$= 22.8 dB. Incident power at normally-oriented (ϕ = 0°) transponder, *OP* = -27 dBm.

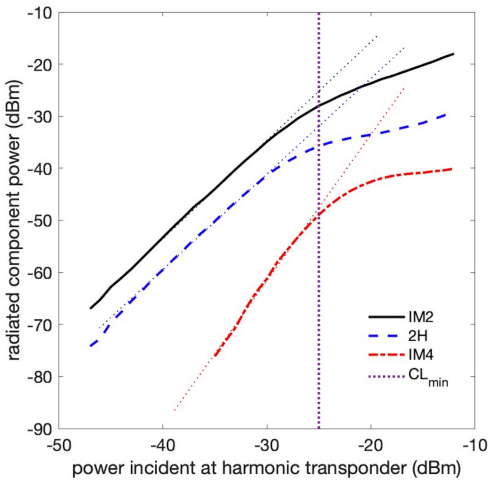

FIGURE 5. Nonlinearity characterization of device seen in Fig. 1. Intermodulation products appearing in the backscattered band (i.e., about 2*f*). Note that the ratio between IM2 and the 2H and IM4 components are depending on the device's *OP*.

ratios depend *only* on the power incident at a normally oriented device, due to interrogator's effective transmit power (known), forward link loss (potentially unknown), and the diode characteristics versus power (known). These ratios do *not* depend at all on the return link (device's transmit antenna, reverse link loss, interrogator's receive antenna).

B. THEORY

The results presented in Fig. 5, particularly the slopes of the curves in the small signal region (i.e., < -25 dBm), are supported by known theory, as we now review in this section.

From Eq. (7), we see the harmonic transponder is interrogated with an equally-weighted two-tone signal. In practice, the power received by the transponder, after link losses, is < -10 dBm. As such, the incident amplitudes of the dual tones, $A < 1$. The output from the nonlinear transponder ($y_{NL}(t)$) is given by Eq. (8). As the conversion loss of different harmonic transponder designs have been shown to range from 3 dB [10] to >20 dB [5], $C_k < 1$ also.

For our purposes, and as shown in Fig. 4, the 2H (i.e., at $2\omega_1$ & $2\omega_2$), IM2 (i.e., at $\omega_1 + \omega_2$), and IM4 (i.e., at $3\omega_1$ - ω_2 & $3\omega_2$ - ω_1) components warrant further exploration. From [20], the 2H component in the small signal region can be expressed as follows,

$$y_{NL(2\omega_{1,2})}(t) = \left(\frac{1}{2}a_2A^2 + 2a_4A^4\right)\cos\left(2\omega_{1,2}t\right),$$

where a_i is a scalar, and since $A < 1$,

$$y_{NL(2\omega_{1,2})}(t) \approx \frac{1}{2}a_2A^2\cos\left(2\omega_{1,2}t\right). \quad (9)$$

The expression for the IM2 components, also from [20], is

$$\begin{aligned} y_{NL(\omega_1+\omega_2)}(t) &= (a_2A^2 + 3a_4A^4)\cos\left((\omega_1+\omega_2)t\right) \\ &\approx a_2A^2\cos\left((\omega_1+\omega_2)t\right). \end{aligned} \quad (10)$$

From Eqs. (9) and (10), we note the ratio of 1/2 between these components and thus would expect an IM2−2H ratio of 3 dB. Our results presented in the following section bear this out, when the incident signal is very small (i.e., < -25 dBm). The final component of interest, IM4, is expressed as

$$y_{NL(3\omega_{1,2}-\omega_{2,1})}(t) = \frac{1}{2}a_4A^4\cos\left((3\omega_{1,2}-\omega_{2,1})t\right). \quad (11)$$

As the second harmonic, second-order IM and fourth-order IM components are individually sinusoids, their output power are respectively given by

$$\begin{aligned} P_{(2\omega_{1,2})} &= \frac{1}{8}a_2^2A^4;\ P_{(\omega_1+\omega_2)} = \frac{1}{2}a_2^2A^4; \\ P_{(3\omega_{1,2}-\omega_{2,1})} &= \frac{1}{8}a_4^2A^8. \end{aligned} \quad (12)$$

The coefficients a_2 and a_4 correspond to the 2H and IM4 components, respectively, and are dependent on the harmonic transponder's diode. From Eq. (12), the slopes of 2H, IM2, and IM4 components are 2, 2, and 3 dB/dB, respectively. These slopes are consistent with the dotted extrapolation shown in Fig. 5. In short, for small signals, theory indicates that the ratio between IM2 and 2H components should change little, whereas the ratio between IM2 and IM4 should change at a rate with magnitude of 1 dB/dB. We will now show additional experimental data that aligns with this theory.

C. RESULTS

To illustrate the proposed interrogation strategy, we continuing leveraging the device seen in Fig. 1. This device has been shown to have a minimum conversion loss of 3 dB, when interrogated at 886.75 MHz, normally oriented, and when the incident power (i.e., *OP*) is −25 dBm [10].

For the empirical data shown next, the device was interrogated, from a distance of 2 m, with two frequencies near 886.75 MHz. Specifically, we set $f_1 = 886.65$ MHz and

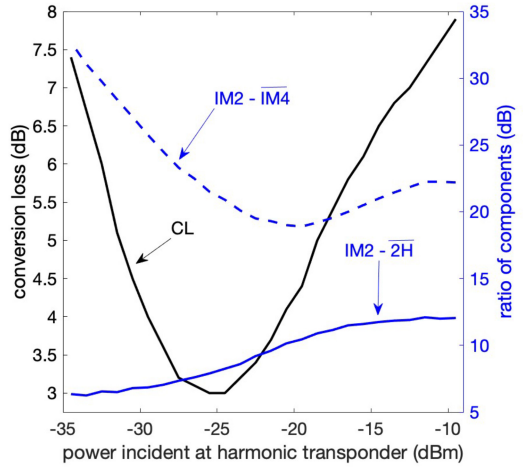

FIGURE 6. Conversion loss of device as a function of incident power (i.e., Operating Point - *OP*), plotted along with the ratio of the IM2 component (i.e., $f_1 + f_2$) to the mean of second harmonics ($\overline{2H}$, i.e., $2f_1$ & $2f_2$) and to the mean of IM4 components ($\overline{IM4}$, i.e., $3f_1 - f_2$ & $3f_2 - f_1$).

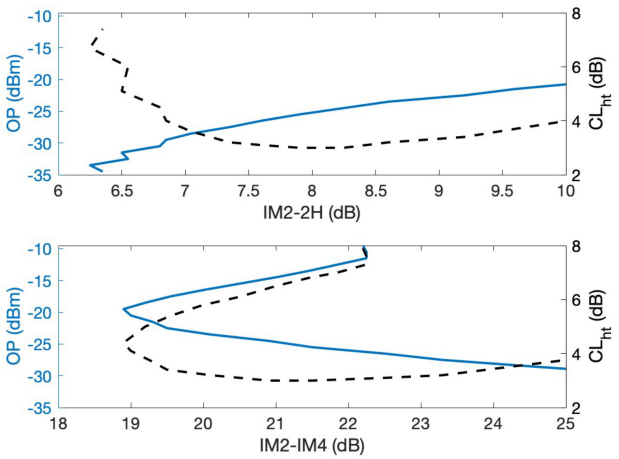

FIGURE 7. Left axis: operating point (OP) of harmonic transponder as a function of the ratio between the IM2 component to the second harmonic (top) and to the IM4 component (bottom). Right axis: harmonic transponder conversion loss (CL_{ht}), with respect to these same parameters.

$f_2 = 886.85$ MHz, using two RF signal generators whose outputs were combined and amplified. Using a spectrum analyzer, the returns in the 1.77 GHz band consisted of the second harmonics (2H) of the interrogation signals and their second- and fourth-order IMDs (IM2 and IM4, respectively), such as shown in Fig. 4.

The transmitted EIRP was then adjusted in 1 dB increments/decrements over a 25 dB range and at each step two measurements were made. The first was a *single*-carrier measurement at $f = 886.75$ MHz, with response measured at $2f$. Eq. (1) can be solved for the device's conversion loss, CL_{ht}, yielding Eq. (13).

$$CL_{ht} = EIRP - P_{I,2f} - L_{fwd,f} - L_{rev,2f} + G_{I,2f} \quad (13)$$

For the test setup, the interrogator's transmit and receive antenna gains ($G_{I,f}$ and $G_{I,2f}$, respectively) are expected to be known. The transmit power is swept, thus the *EIRP* is set. For freespace testing, path losses ($L_{fwd,f}$ and $L_{rev,2f}$) can be calculated from the Friis equation. As such, the device's CL_{ht} can be found readily by measuring the backscattered power ($P_{I,2f}$). These data are plotted using the left y-axis of Fig. 6 (conversion loss).

The second measurement leverages the dual frequency approach described in Section IV-A. Using a spectrum analyzer, the power of the five distinct frequencies, such as seen in Fig. 4, were measured. Note that there are *two* second harmonic (2H) components and *two* fourth-order intermodulation (IM4) components. As such, we consider the *single* IM2 component ($f_1 + f_2$) as the reference for calculating the ratios between these distortion products. Specifically, we quantify the ratio between the IM2 component and the *mean* of the two second harmonic components ($\overline{2H}$), and the ratio between the IM2 component and the *mean* of the two IM4 components ($\overline{IM4}$). For an *OP* dynamic range of 25 dB, these ratios (differences in dB) for IM2-$\overline{2H}$ and IM2-$\overline{IM4}$ are plotted in Fig. 6 (the right y-axis provides the scale).

Consistent with the theory presented in the previous subsection, we see for the small signal region (i.e., < -25 dBm) that the IM2-$\overline{2H}$ ratio is $\sim$3 dB and that the IM2-$\overline{IM4}$ ratio changes with slope -1 dB/dB. Note also that the IM2-$\overline{IM4}$ curve is not monotonic. However, by using the IM2-$\overline{2H}$ curve, one can resolve the region the device is operating in. In short, with these three well-behaved curves, one can readily solve the inverse problem in which one has measured IM product ratios in order to determine the *OP* and conversion loss of the device.

Fig. 7 shows this inverse mapping, where the these measurable ratios can provide the device's operating point (*OP*, left y-axis) and conversion loss (CL_{ht}, right y-axis). As an example, consider the measured data shown in Fig. 4, from which the following ratios can be found: IM2-$\overline{2H}$= 7.6 dB and IM2-$\overline{IM4}$= 22.8 dB. Using Fig. 7$-$*top*, the IM2-$\overline{2H}$ ratio corresponds to an interpolated *OP* of -26.5 dBm, while using Fig. 7$-$*bottom*, the measured IM2-$\overline{IM4}$ ratio results in an interpolated *OP* of -26.9 dBm. Both results are within 0.5 dB of the actual -27 dBm incident power.

These results indicate that over a 25 dB range, and using an OTA approach, the incident power at a *remote* harmonic transponder can be found with good accuracy using *only* the signals measured at the interrogator. In the next section, we illustrate one possible application for this methodology.

V. EXAMPLE APPLICATION: OTA CHARACTERIZATION

While the performance of harmonic transponder's receive and transmit antennas, and diode, can be *separately* characterized *prior* to the device's assembly, this is not the case after integration of these three components. Changes from these individual component measurements can occur due to, e.g., impedance mismatch between either/both antennas and the diode [10], antenna pattern deformation caused by the object the device is deployed on (e.g., human body [21]), or by the media the device is deployed in (e.g., soil [22]).

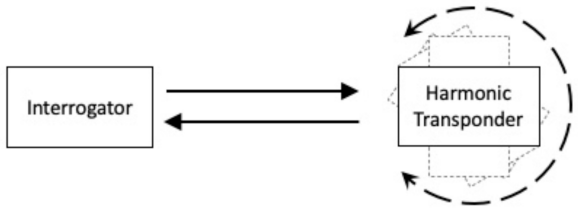

FIGURE 8. Test setup for proposed harmonic transponder antenna mapping.

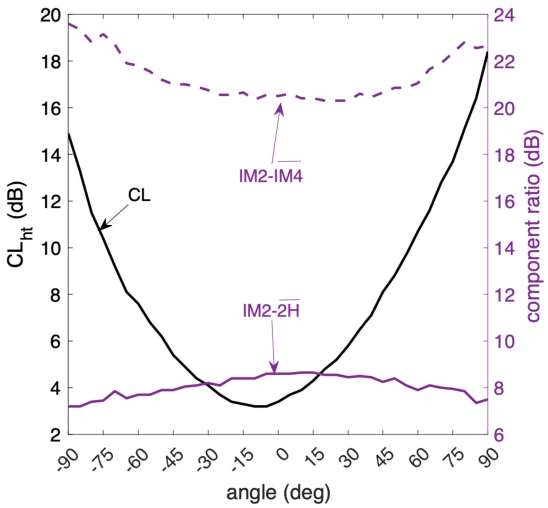

FIGURE 9. Device conversion loss (CL_{ht}, left axis) and component ratios (right axis) as a function of azimuth angle.

As such, being able to characterize *in situ* a fully-integrated and deployed transponder would be of interest.

To illustrate how such measurements might be possible, we consider the scenario of conducting OTA laboratory measurements on the fully-assembled transponder seen in Fig. 1, over azimuth angle (ϕ). As illustrated in Fig. 8, a harmonic transponder was placed on rotating platform. With the interrogation *EIRP* fixed throughout the test, the device was rotated to different positions, as would be done with any antenna azimuth pattern test. The *EIRP* used in this testing corresponds to -27 dBm at the harmonic transponder, when normally oriented (i.e., $\phi = 0°$). That is, the test conditions leading the response shown in Fig. 4.

As device rotates away from its normal orientation, two things will occur. First, the absolute power of the signal received by the interrogator can be expected to change. This will be due to (i) changing gain from the device's receive antenna ($G_{ht,f}$) as a function of angle, causing (ii) a change in the power incident at the transponder's diode, thereby causing a change in the diode's conversion (CL_d), and finally, (iii) changing gain as a function of angle from the device's transmit antenna ($G_{ht,2f}$).

Second, changing the incident power at the diode causes its nonlinear characteristics to change, which impacts the measurable IMD ratios. We present such data in Fig. 9. The left y-axis shows the single frequency conversion loss. As

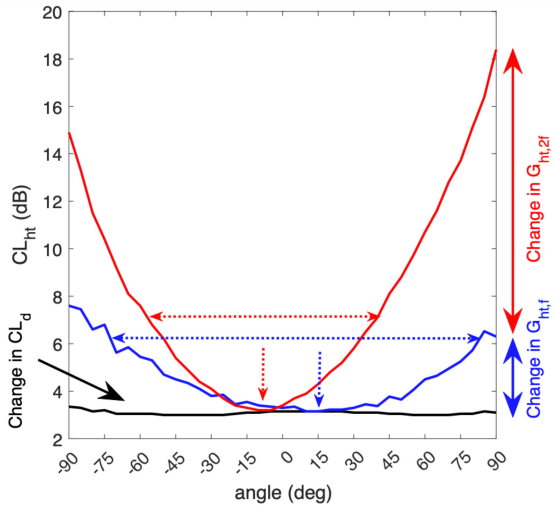

FIGURE 10. Total device conversion loss over azimuth data decomposed by the relative contribution of the transponder's receive antenna gain pattern, transmit antenna gain pattern, and diode conversion loss.

would be expected, as the device is rotated from the receive and transmit peak-of-beams orientation, the conversion loss increases *relative* to that for its normal orientation.

The right y-axis shows the IM2-$\overline{2H}$ and IM2-$\overline{IM4}$ ratios over azimuth angle, indicating decreasing and increasing values, respectively, over angle. These data, along with Fig. 7, can be used to determine the change in *OP* relative to $\phi = 0°$. Any variation in IMD ratios from the baseline measurement (i.e., at angle 0°), will only be due to a change in the device's receive antenna pattern, $G_{ht,f}$. Any change in the diode's conversion loss can be found from knowing this change in the effective *OP*. Fig. 10 plots these individual changes. We note that the $G_{ht,f}$ (blue trace) degrades $\sim$3$-$4 dB over the $\pm$90° azimuth sweep. This variation increases the total conversion loss $\sim$0.5 dB, but only at the edge of the pattern (black trace).

Any remaining change in the total conversion loss is due solely due to changes in the device's transmit antenna pattern ($G_{ht,2f}$) with angle, which can be calculated using Eq. (14). From our transponder test, we show this change in gain also in Fig. 10 (red trace).

$$G_{ht,2f} = \underbrace{P_{I,2f}}_{\text{measured}} + \underbrace{G_{I,2f} - L_{ref,2f}}_{\text{known}} + \underbrace{OP}_{IMD\ \text{data}} - \underbrace{CL_d}_{CL\ \text{data}} \tag{14}$$

Marked on Fig. 10 are both the pattern center points and 3 dB beamwidths. From these data, we see slight shifts between the receive and transmit patterns.

Simulation results for this transponder (from [5]), separately considered the receive and transmit antennas at 867 MHz. We present these simulated azimuth patterns (with gains normalized) in Fig. 11, along with our deconstructed patterns, with the beam peaks aligned to 0°. The 3 dB beamwidth for the receive antenna is $\sim$155°, versus $>$180°

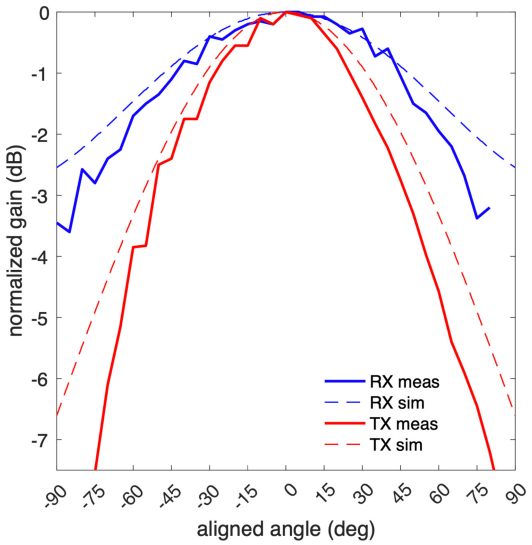

FIGURE 11. Comparison of decomposed transponder transmit and receive antenna gains with design simulations from [5].

provided by simulation. Similarly, we measured ∼100° for the 3 dB transmit beamwidth, slightly narrower that the ∼113° noted in simulation. While these results are not exact to what were simulated, potentially due to measurements being conducted at a higher frequency, they represent data for the fully integrated device and illustrate performance that is not unexpected for the given design. In short, using the IMD ratio approach, we are able to deconstruct, using remote over-the-air measurements, the individual contributions of the transponder's three distinct components to the device's overall conversion loss.

Like any OTA measurement, the uncertainty associated with a single power measurement is non-zero. However, based on the data presented in Fig. 10, the *OP* recovered from the two IM ratios (i.e., IM2-$\overline{2H}$ and IM2-$\overline{IM4}$) are consistently within ±1 dB of each other, over the full range of azimuth measurements made. The implication is that from a *single* two-tone measurement, the IM ratios can be used to determine the device's *OP* within ±1 dB. This uncertainty is well within that reported for other OTA measurement campaigns [23]. From the *OP*, the device's conversion loss can be directly and accurately found (e.g., within ±0.25 dB) using, in our work, Fig. 6 or Fig. 7. In contrast, a single-tone approach would require *multiple* measurements to ascertain the device's *OP*. Using Fig. 6, we find the reasons are two-fold. First, conversion loss is not a monotonic function. Thus with a single *CL* measurement, one can not uniquely determine the *OP*. Second, conversion loss varies little with *OP* in the region of CL_{min}. As such, a single *CL* measurement, with its potential error, could translate into a significant range of *OP*s. For example and using our data from Fig. 6, a single-carrier measurement that results in a range of *CL* from 3 dB to 4 dB (i.e., ±0.5 dB OTA measurement error), could translate to *OP*s ranging from −20 dBm to −30 dBm.

The presented device decomposition example illustrates that, by using the presented IMD ratio method, we can *accurately* and *separately* isolate the signal changes at the interrogation frequency, f, from the signal changes at the backscattered frequency, $2f$, while also accounting for any nonlinearity produced by the diode. This demonstration is a surrogate for showing that if a harmonic transponder were embedded within an unknown media, then the approach could be used to *separately* determine channel losses at f *and* at $2f$. Having two loss measurements at two different frequencies for the same channel, could be advantageous for applications, e.g., sensing soil moisture with a buried harmonic transponder.

VI. CONCLUSION

In this work, we have presented an approach to interrogating harmonic transponders, with the objective of being able to find operating point (*OP*) of the device, once it has been fully assembled and deployed in the field. We have shown, using empirical data, that the ratios between the intermodulation distortion products produced when interrogating with two, close-spaced frequencies will change in a well-behaved manner with changes in this *OP*. Our initial results indicate that the *OP* can be remotely determined with accuracy of within ±1 dB, over a 25 dB dynamic range. This result is respectable when compared to OTA power measurements made for other devices and applications.

We have also presented a possible application for the proposed approach, i.e., characterizing a fully integrated transponders using an OTA approach. Other applications is to use an embedded transponder to characterize forward and reverse channel losses. This could have applications for, e.g., monitoring soil moisture, an application under current investigation.

ACKNOWLEDGMENT

The authors wishes to thank Milan Polívka for discussions about this work. The authors also wish to thank Isabel Nerad for assistance in data collection.

REFERENCES

[1] A. Lavrenko, B. Litchfield, G. Woodward, and S. Pawson, "Design and evaluation of a compact harmonic transponder for insect tracking," *IEEE Microw. Wireless Compon. Lett.*, vol. 30, no. 4, pp. 445–448, Apr. 2020.

[2] M. I. M. Ghazali, S. Karuppuswami, and P. Chahal, "3-D printed embedded passive harmonic sensor tag as markers for buried assets localization," *IEEE Sensor Lett.*, vol. 3, no. 4, pp. 1–4, Apr. 2019.

[3] X. Gu, K. Wu, and S. Hemour, "Remote temperature sensing based on battery-free harmonic backscattering," in *Proc. IEEE Int. Symp. Antennas Propagat. North Am. Radio Sci. Meeting*, 2020, pp. 1429–1430.

[4] A. Lazaro, R. Villarino, and D. Girbau, "A passive harmonic tag for humidity sensing," *Int. J. Antennas Propagat.*, vol. 2014, no. 1, 2014, Art. no. 670345.

[5] M. Polivka, V. Hubata-Vacek, and M. Svanda, "Harmonic balance/full-wave analysis of wearable harmonic transponder for IoT applications," *IEEE Trans. Antennas Propag.*, vol. 70, no. 2, pp. 977–987, Feb. 2022.

[6] I. T. Nassar and T. M. Weller, "A compact dual-channel transceiver for long-range passive embedded monitoring," *IEEE Trans. Microw. Theory Techn.*, vol. 63, no. 1, pp. 287–294, Jan. 2015.

[7] I. T. Nassar, T. M. Weller, and J. L. Frolik, "A compact 3-D harmonic repeater for passive wireless sensing," *IEEE Trans. Microw. Theory Techn.*, vol. 60, no. 10, pp. 3309–3316, Oct. 2012.

[8] J. Frolik, J. E. Lens, M. M. Dewoolkar, and T. M. Weller, "Effects of soil characteristics on passive wireless sensor interrogation," *IEEE Sensors J.*, vol. 18, no. 8, pp. 3454–3460, Apr. 2018.

[9] K. Rasilainen and V. V. Viikari, "Transponder designs for harmonic radar applications," *Int. J. Antennas Propagat.*, vol. 2015, Sep. 2015, Art. no. 565734.

[10] M. Poliva and J. Frolik, "On performance characterization of harmonic transponders," *IEEE Open J. Antennas Propagat.*, vol. 5, pp. 37–45, 2024.

[11] M. Ritämaki, A. Ruhanen, V. Kukko, J. Miettinen, and L. H. Turner, "Contactless radiation pattern measurement method for UHF RFID transponders," *Electron. Lett.*, vol. 41, no. 13, p. 1, Jul. 2005.

[12] J.-M. Hannula, K. Rasilainen, and V. Viikari, "Characterization of transponder antennas using intermodulation response," *IEEE Trans. Antennas Propag.*, vol. 63, no. 6, pp. 2412–2420, Jun. 2015.

[13] M. Polivka and J. Frolik, "Characterizing harmonic transponder performance jointly over frequency and power," in *Proc. 17th Eur. Conf. Antennas Propagat.*, 2023, pp. 1–5.

[14] T. Rappaport, *Wireless Communications—Principles and Practice*. Hoboken, NJ, USA: Prentice Hall, 1996.

[15] F. Ulaby, R. Moore, and A. Fung, *Microwave Remote Sensing*. Norwood, MA, USA: Artech House, 1986.

[16] D. K. Goot, H. Chaubey, T. Y. Hsu, and W. S. Deal, "A perceptual evaluation of music real-time communication applications," *IEEE Access*, vol. 11, pp. 46860–46870, 2023.

[17] *IEEE Recommended Practices and Requirements for Harmonic Control in Electrical Power Systems*, IEEE Standard 519-2022, 2022.

[18] *Test Procedure for Measuring the 3rd Order Intercept Point (IP_3) Level of Radio Monitoring Receivers*, ITU-Rec. SM.1837-1, Int. Telecommun. Union, Geneva, Switzerland, 2013.

[19] N.-C. Kuo, B. Zhao, and A. M. Niknejad, "Intermodulation uplink for far-field passive RFID applications," in *Proc. IEEE/MTT-S Int. Microw. Symp.*, 2018, pp. 274–277.

[20] X. Yang, S. Li, and F. Li, "Fourth-order nonlinear distortion to the power spectrum of RF amplifiers," *J. Eng.*, vol. 2022, no. 1, pp. 53–63, 2022.

[21] J. Frolik and M. Polivka, "Impact of bodies on harmonic transponder conversion loss and radiation patterns," in *Proc. IEEE Int. Symp. Antennas Propag. USNC-URSI Radio Sci. Meeting (USNC-URSI)*, 2023, pp. 1339–1340.

[22] H. Zemmour, G. Baudoin, C. Hamouda, A. Diet, and M. Biancheri-Astier, "Impact of soil on UWB buried antenna and communication link in IR-UWB WUSN applications," in *Proc. Eur. Radar Conf. (EuRAD)*, 2015, pp. 353–356.

[23] P. Shen, Y. Qi, W. Yu, J. Fan, and F. Li, "OTA measurement for IoT wireless device performance evaluation: Challenges and solutions," *IEEE Internet Things J.*, vol. 6, no. 1, pp. 1223–1237, Feb. 2019.